# Assessing the Performance of Density Functional Theory for the Electronic Structure of Metal−Salens: The $3d^0$-Metals

**John S. Sears and C. David Sherrill***

*Center for Computational Molecular Science and Technology, School of Chemistry and Biochemistry, Georgia Institute of Technology, Atlanta, Georgia 30332-0400*

*Received: December 9, 2007; In Final Form: February 1, 2008*

A series of metal−salen complexes of the $3d^0$ metals Sc(III), Ti(IV), V(V), Cr(VI), and Mn(VII) have been explored using high-level electronic structure methods including coupled-cluster theory with singles, doubles, and perturbative triples as well as complete active-space third-order perturbation theory. The performance of three common density functional theory approaches has been assessed for both the geometries and the relative energies of the low-lying electronic states. The nondynamical correlation effects are demonstrated to be extremely large in all of the systems examined. Although density functional theory provides reasonable results for some of the systems, the overall agreement is quite poor. This said, the density functional theory approaches are shown to outperform the single-reference perturbation theory and coupled-cluster theory approaches for cases of strong nondynamical correlation.

## Introduction

Jacobsen has referred to complexes of salen [bis(salicylaldehydo)ethylenediamine] and salen-type ligands as "privileged catalysts",[1] and such ligands certainly comprise one of the most important classes of synthetic ligand systems in the context of homogeneous catalysis.[2−4] Complexes of 3d- and 4d-transition metals with salen or salen-like ligands have seen numerous applications in homogeneous asymmetric catalysis.[5−7] Furthermore, the stability of metal−salen complexes makes them interesting targets for immobilzation. It has been demonstrated that different immobilization schemes may greatly impact the catalytic activity of immobilized molecular catalysts,[8] and the design of an appropriate immobilization scheme can be greatly aided by knowledge of the underlying catalytic mechanism. While the development of improved immobilized salen catalysts could be greatly assisted by theoretical insight, theoretical studies of metal−salen catalysts have been somewhat limited. Indeed, with the exception of the Mn(salen) catalysts that have been so extensively studied over the preceding decade,[9−25] few metal−salen systems have seen extensive theoretical investigation.[12,26] This is in no small part a consequence of the discrepancies that were revealed for the Mn(salen) systems when using two of the most common density functional theory (DFT) methods.[22] Indeed, recent work in our group has highlighted the difficulties in applying conventional methods of electronic structure theory to particular metal−salen systems.[27]

The rapid advances in computational abilities and methods increasingly make new, and more challenging, systems available to the theoretical and computational chemists. However, as pointed out by Davidson in 1991:[28] "The theory of transition-metal chemistry has lagged behind the quantum theory of organic chemistry because quantitative wave functions are more complicated." The development of DFT[29,30] and its introduction into the mainstream theoretical community has undoubtedly transformed the field over the previous decade. The applicability of DFT methods to much larger systems and its successful applications in organic chemistry have made DFT methods, quite often, the method of choice for computational chemists. While the remarkable success of DFT methods has attracted many,[31] the reliability of DFT methods for mixed organic−inorganic systems remains an open question.[32] While benchmark studies of DFT methods for transition-metal systems exist, these have been limited to metal ions,[33] to transition-metal homo-[34,35] and heterodimers,[36,37] and to systems with a limited number of small ligands.[38−40] While certainly useful in their own regard, such benchmarks neglect the differing character of the bonding in such systems and of that in the saturated or nearly saturated metal−ligand systems that are of the most chemical interest (such as in metal−ligand catalyst systems). Furthermore, recent work indicates that systematic errors in popular DFT methods may become increasingly problematic as the size of the system increases.[41]

In an effort to ascertain the reliability of DFT for exploring metal−salen chemistry, we examine the electronic structure of a series of $3d^0$ metal−salens [Sc(III), Ti(IV), V(IV), Cr(VI), and Mn(VII)] using high-level *ab initio* methods as benchmarks. Possessing an empty 3d-shell, it is anticipated that the $d^0$-metal salens will be the most well described by single-reference approaches of all the metal−salen systems. Although the goal of this work is to benchmark results from DFT against reliable *ab initio* data and not to directly explore the chemistry of any particular experimentally employed metal−salen catalysts, it should be noted that many $d^0$-metal salens have been synthesized for metal−salen-catalyzed reactions. Sc(III)−salens have been employed as highly efficient catalysts for Diels−Alder reactions.[42,43] Ti(IV)−salens have seen extensive use as catalysts for asymmetric ring-opening,[44−46] while Ti(IV)− and V(V)−salens have been routinely employed as catalysts in cyano-addition reactions.[47−53] The ability of electronic-structure methods to reliably model metal−salen catalyzed chemical transformations will open the doorway to the theoretical exploration and the understanding of varied and numerous catalytic pathways.

* Corresponding author. E-mail: sherrill@gatech.edu.

10.1021/jp711595w CCC: $40.75 
Published on Web 03/14/2008

## Computational Methods

All DFT computations were performed with Jaguar 5.5.[54] The computations were performed using three of the most common combinations of exchange and correlation functionals: the combination of Becke's 1988 exchange functional[55] with Perdew's 1986[56] functional for correlation referred to as BP86, the combination of Becke's 1988 exchange functional with the Perdew−Wang 1991 functional for correlation[57] referred to as BPW91, and the combination of Becke's three-parameter hybrid functional[58] with the correlation functional by Lee, Yang, and Parr[59] referred to as B3LYP. Unless otherwise stated, all DFT computations employed the pseudospectral implementation of DFT[60] and a fine grid as found in Jaguar 5.5, and the Los Alamos basis-sets and corresponding effective core potentials of Hay and Wadt (LANL2DZ) for all transition-metal atoms[61] and a 6-31G* basis for all other atoms.[62] Geometries were completely optimized (rms gradient $10^{-3}$) without symmetry for the lowest singlet, triplet, and quintet states using each functional. The nature of the stationary points was verified by computing analytic frequencies.

Geometries were also optimized (rms gradient $10^{-3}$) at the second-order Møller−Plesset perturbation theory (MP2)[63] level with ACES II[64] and the complete active-space self-consistent field (CASSCF)[65] level with MOLPRO 2006.1.[66] Unless otherwise stated, the converged BP86 geometries were employed as a starting point for these optimizations. Active spaces for CASSCF computations were chosen by examination of the configuration interaction (CI) vector from large CAS-CI[67] computations performed in a configuration interaction singles and doubles (CISD)[67] natural orbital (NO) basis. Starting orbitals for the CASSCF computations were generated from CASSCF NO's computed in the smaller STO-3G[68−70] basis. The STO-3G CASSCF computations employed a CISD NO guess. Such an approach has been shown to give reliable convergence for CASSCF computations on other metal−salen systems, when more conventional approaches have failed to do so.[27] The active spaces and optimized states for each system will be described in the discussion, employing the notation from our previous work.[27] Single-point energies were computed at the MP2-optimized geometries using coupled-cluster theory including single and double excitation operators (CCSD)[71] and perturbative triples (CCSD(T))[72] with MOLPRO 2006.1. Single-point energy corrections were computed at the CASSCF-optimized geometries at the complete active-space second-order and third-order perturbation theory (CASPT2[73,74] and CASPT3[75]) with MOLPRO 2006.1. Because of limitations on the number of correlated orbitals in the CASPT3 program, CASPT3 computations were carried out with the lowest $\sigma$-orbitals frozen and combined as corrections to the internally contracted CASPT2 results. All wavefunction-based computations employed a 6-31G* basis and the frozen-core approximation using a small core, defined as 1s2s2p3s for first transition-row metals.

Optimized geometries were compared and the least root-mean-squared deviations (LRMSD) in molecular geometries were computed using the visual molecular dynamics (VMD) program.[76] Molecular orbital isosurfaces were generated (contour value of 0.05) using MOLEKEL.[77] Numerous diagnostics to ascertain the multireference character of the wave function based upon amplitudes from MP2 or CCSD calculations have been developed.[78−83] To assess the multireference character of the electronic states in $3d^0$-metal salens, we report two of the most commonly employed diagnostics: the T1-diagnostic[78] and the D1-diagnostic[83] from the converged CCSD computations. The T1-diagnostic, based upon the Euclidian norm of the $t_1$ vector from a CCSD calculation, provides information about the average magnitude of the singles amplitudes while the D1-diagnostic, based upon the 2-norm of the $t_1$ vector, provides information about the largest singles amplitudes. As suggested by Lee,[79] we have also examined the ratio of the T1-diagnostic and the D1-diagnostic. As Lee points out,[79] "the T1/D1 ratio itself does not indicate how well the coupled-cluster approach is performing—it is only a measure of the molecular electronic structure homogeneity." Lee demonstrates that in a completely homogeneous system the ratio (T1/D1) tends to $1/\sqrt{2}$ and that in molecular systems it will deviate from the value by becoming less than $1/\sqrt{2}$. When T1/D1 is small, this is an indication that there is a large variation in the orbital rotation parameters. Additional information about the multireference nature of the electronic states has been provided by examination of the leading determinants (and coefficients) from the CASSCF CI expansions.

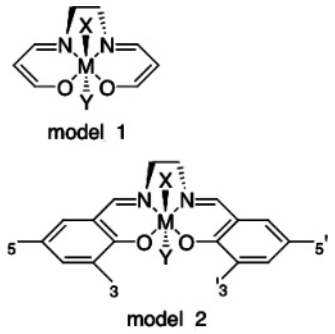


**Figure 1.** Two of the most common model systems for metal−salen catalysts.

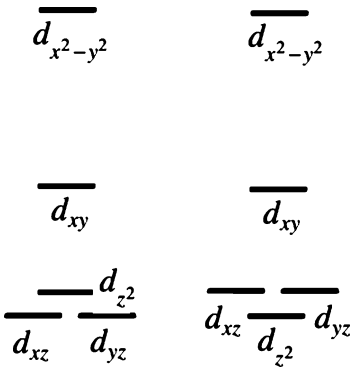

**Figure 2.** Two commonly presented d-orbital splitting diagrams for a square-planar coordination geometry.

## Results and Discussion

Two of the common model systems employed in previous theoretical studies of metal−salen systems are depicted in Figure 1. While model 2 most nearly delineates the full salen ligand and has been employed in limited studies by previous authors, the truncated model 1 has certainly been the most routinely applied in previous theoretical studies of metal−salen complexes. Given that the truncated model 1 is the most routinely applied in theoretical investigations, this work examines the low-lying electronic states for the systems of the form model 1 [X = none, Y = none, M ∈ {Sc(III), Ti(IV), V(V), Cr(VI), Mn-(VII)}]. None of the M(salen) complexes studied contain any symmetry elements, and therefore all calculations were performed in $C_1$ symmetry. The salen ligand does, however, form a pseudo-square-planar coordination sphere around the central metal atom.

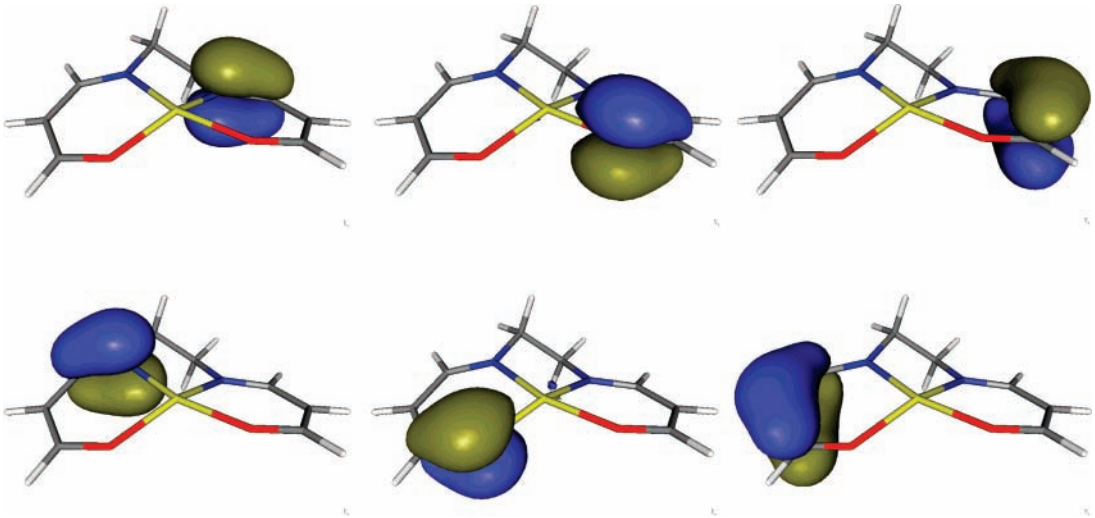

**Figure 3.** Figure of the localized CN-$\pi$ (left), CO-$\pi$ (center), and three-center−two-electron R$\pi$ orbitals (right) of the salen ligand from a HF/6-31G* calculation of the singlet state of Sc(III)−salen.

The selection of appropriate active spaces for the construction of the CASSCF wave functions requires a certain amount of chemical insight, thus it is useful to consider the important properties of the electronic structure of metal−salen systems before proceeding further. The four coordinating atoms [O,N,N,O] induce a well-known splitting of the metal d-orbital energy levels. Two typical d-orbital splitting diagrams for square-planar coordination presented in the literature are displayed in Figure 2. The degenerate (nearly degenerate for the case of nonsymmetrical coordination) $d_{xz}$ and $d_{yz}$ orbitals are considered to be the lowest in energy and this is typically true in the weak-field case. The $d_{xz}$ and $d_{yz}$ orbitals are followed closely by the $d_{z^2}$ orbital, and these are energetically well separated from the $d_{xy}$ and the much higher lying $d_{x^2-y^2}$ orbitals. Strong ligand fields, mixing of the *s* and $d_{z^2}$ orbitals, or strong metal−ligand covalency have been shown to result in a flipping of the ordering of the $d_{xz}$ and $d_{yz}$ orbitals and the $d_{z^2}$ orbital.[84−86] This splitting will play heavily into the construction and interpretation of the active spaces discussed below, as the metal d-orbitals most likely to contribute to the electronic structure will be the low-lying $d_{xz}$, $d_{yz}$, and $d_{z^2}$ orbitals. To ascertain the important electronic effects of the salen ligand and further examine the chemistry taking place in the metal−salen systems, RHF/6-31G* wave functions were constructed (consisting of 54 doubly occupied molecular orbitals) at the BP86 $1^1$A optimized geometries and the occupied orbitals were localized via Edmiston−Ruedenberg (ER) localization.[87] The anticipated $\sigma$ bonds occurring in the salen ligand are observed along with the N and O lone pairs involved in dative bonding with the central metal atom. Each O atom has an additional lone pair that is not involved in any bonding interactions. The most important feature observed for the electronic structure is the presence of six $\pi$-type orbitals on the salen ligand: two representing C−O $\pi$ bonds, two representing C−N $\pi$ bonds, and two C−C−C (three-center-two-electron) $\pi$ bonds hereafter referred to as R$\pi_1$ and R$\pi_2$. These are displayed in Figure 3 from the ER localized orbitals of Sc(III)−salen. Given the absence of metal d electrons for the systems studied here (at least in the formal oxidation state picture) it is anticipated that the low-lying electronic states will be dominated by the closed-shell electronic configuration and either ligand $\pi \rightarrow \pi^*$ excitations or $\pi \rightarrow$ d ligand-to-metal excitations, the latter becoming increasingly important as the formal oxidation state of the metal center is increased. The construction and interpretation of the active space for each system and the nature of the low-lying electronic states will be discussed in detail in the following sections.

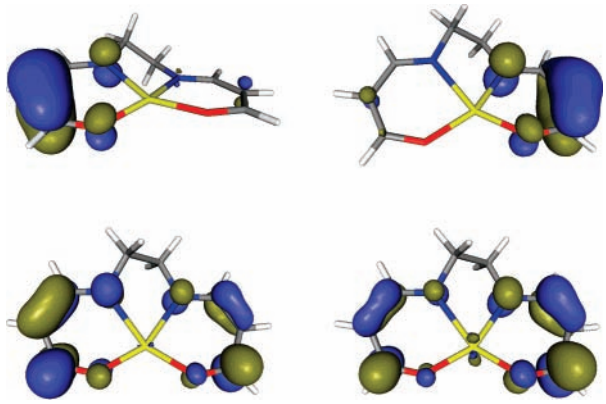

**Figure 4.** Isosurface plots of the R$\pi_1$ (upper left), R$\pi_2$ (upper right), CN/CO$\pi^*_1$ (lower left), and CN/CO$\pi^*_2$ (lower right) orbitals that comprise the active space for Sc(III)−salen.

**Sc(III)—Salen.** It is not completely clear a priori, given that Sc(III)−salen is anticipated to be strongly single-reference, whether CCSD(T) or CASPT3 will provide more reliable relative energies. CAS−CI calculations including 12 electrons in 12 molecular orbitals reveal the closed-shell singlet ground state and two nearly degenerate (and highly multireference) triplet states. All states appear well described by an active space consisting of four electrons in four spatial orbitals. The geometries of these states were optimized at the SA-CASSCF-(4/4)/6-31G*[$1^1$A,$1^3$A,$2^3$A,$1^5$A] level of theory, where the states in brackets are those included in the state averaging. The SA-CASSCF NO's from the optimized $1^3$A state are depicted in Figure 4. The relative energies from all *ab initio* calculations are included in Table 1. Both CASPT3 and CCSD(T) predict a closed-shell ground state, with the first triplet state slightly more than 60 kcal mol$^{-1}$ higher in energy. The quintet is observed at slightly less than 130 kcal mol$^{-1}$. From Table 1 it is clear that both the CCSD(T) and CASPT3 methods provide similar relative energies for the lowest electronic states of Sc(III)−salen.

For Sc(III)−salen, all DFT calculations predict a closed-shell singlet ground state well separated from the lowest triplet and quintet states. The relative energies from all DFT are included in Table 1. As has been observed in other metal−salen system,[27] the DFT relative energies are much less sensitive to the choice

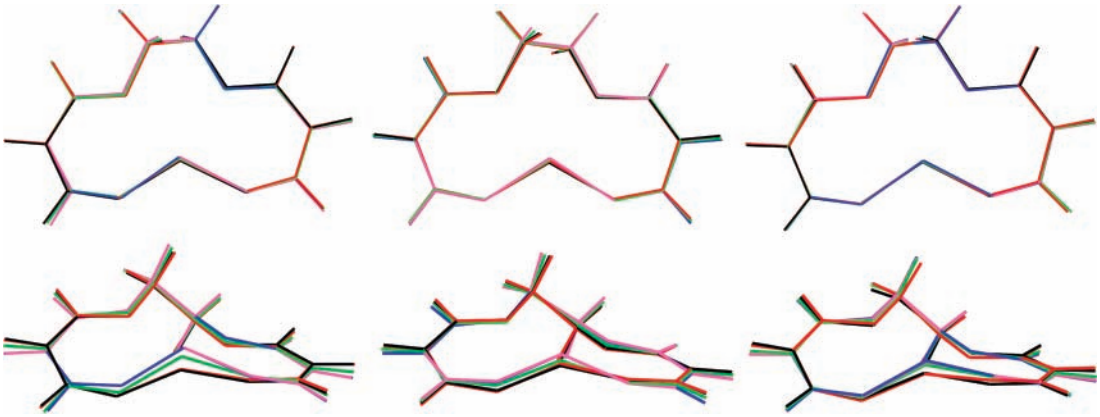

**Figure 5.** Overlay of the optimized geometries for the $1^1$A (left), $1^3$A (center), and $1^5$A (right) states of Sc(III)−salen from different levels of theory. The theoretical methods include CASSCF (black), MP2 (red), B3LYP (green), BP86 (blue), and BPW91 (mauve).

**TABLE 1: Relative Energies (kcal mol$^{-1}$) for the Low-Lying Electronic States of Sc(III)−Salen Computed at Various Levels of Theory**

| | CASPT3[a] | CASPT2[a] | CASSCF | CCSD(T)[b] | CCSD[b] | MP2 | B3LYP | BP86 | BPW91 |
|---|---|---|---|---|---|---|---|---|---|
| $1^1$A | 0.00 | 0.00 | 0.00 | 0.00 | 0.00 | 0.00 | 0.00 | 0.00 | 0.00 |
| $1^3$A | 64.44 | 58.36 | 66.17 | 62.98 | 62.30 | 65.13 | 52.84 | 48.00 | 47.91 |
| $2^3$A | 82.23 | 77.32 | 66.17 | | | | | | |
| $1^5$A | 129.16 | 117.56 | 132.99 | 126.59 | 125.19 | 130.67 | 109.85 | 104.78 | 104.51 |

[a] Relative energies computed at the CASSCF optimized geometries. [b] Relative energies computed at the MP2 optimized geometries.

**TABLE 2: LRMSD(Å) in Molecular Geometries for the $1^1$A, $1^3$A, and $1^5$A States of (Lower Triangular) Sc(III)− and (Upper Triangular) Ti(IV)−Salens**

| | | CASSCF | MP2 | B3LYP | BP86 | BPW91 | | |
|---|---|---|---|---|---|---|---|---|
| | CASSCF | --- | | | | | CASSCF | |
| | | --- | | | | | | |
| | | --- | | | | | | |
| | MP2 | 0.049 | --- | 0.113 | 0.103 | 0.125 | MP2 | |
| | | 0.043 | --- | 0.301 | 0.359 | 0.358 | | |
| | | 0.097 | --- | 0.343 | 0.279 | 0.287 | | |
| Sc(III) | B3LYP | 0.140 | 0.130 | --- | 0.037 | 0.027 | B3LYP | Ti(IV) |
| | | 0.093 | 0.122 | --- | 0.081 | 0.086 | | |
| | | 0.125 | 0.131 | --- | 0.079 | 0.070 | | |
| | BP86 | 0.246 | 0.247 | 0.125 | --- | 0.028 | BP86 | |
| | | 0.184 | 0.211 | 0.099 | --- | 0.025 | | |
| | | 0.172 | 0.176 | 0.051 | ---- | 0.011 | | |
| | BPW91 | 0.246 | 0.245 | 0.123 | 0.004 | --- | BPW91 | |
| | | 0.188 | 0.214 | 0.103 | 0.006 | --- | | |
| | | 0.169 | 0.172 | 0.047 | 0.009 | --- | | |

of correlation functional than to the choice of exchange functional; the results from BP86 and BPW91 are nearly identical. Somewhat surprisingly, B3LYP predicts larger high-spin/low-spin splittings than the nonhybrid approaches. B3LYP (as a consequence of the HF exchange) is known to overstabilize high-spin states in other metal−salen systems when compared to nonhybrid functionals.[27] Although the B3LYP results are somewhat closer to those from CASPT3 and CCSD(T), all functionals provide a consistent picture of the electronic structure for Sc(III)−salen: a singlet ground state followed by the triplet state at approximately 50 kcal mol$^{-1}$ and the quintet state at slightly more than 100 kcal mol$^{-1}$.

The optimized geometries of the $1^1$A, $1^3$A, and $1^5$A states from DFT, MP2, and CASSCF are overlaid in Figure 5 and the LRMSD's in molecular geometries are tabulated in Table 2. The CASSCF and MP2 geometries are very similar for all states (LRMSD < 0.1Å). As has been observed with the relative energies above, the geometries from DFT appear highly insensitive to the choice of correlation functional. The geometries from BP86 and BPW91 are nearly indistinguishable (LRMSD < 0.01Å). One noticeable trend in the geometries is that the amount of "exact" exchange appears to have an effect on the out-of-plane puckering of the Sc(III) center. The MP2 and CASSCF geometries predict a nearly planar geometry while the BP86 and BPW91 geometries predict the Sc(III) center to be slightly distorted out of the ring. The B3LYP geometry lies somewhere in between, with the Sc center out of the plane but not to the extent predicted by the nonhybrid functionals. Overall, B3LYP more closely reproduces the *ab initio* geometries with a maximum LRMSD of 0.140Å.

One of the central concerns related to the applicability of DFT to these systems is the multireference nature of the electronic states. The diagnostics from CCSD calculations are tabulated in Table 3, and the leading determinants in the CASSCF description of the electronic states are tabulated in Table 4. From Table 3 we observe that the T1 diagnostics are slightly larger than typically accepted cutoff values (0.020 and 0.025 for closed- and open-shell systems respectively[78,81,83]) although it should be noted these cut-offs are based upon previous studies of small diatomic and polyatomic systems of first- and second-row atoms.[78−83] There have been limited applications of the T1- and D1-diagnostics to large transition-metal containing systems and the values observed from Table 3 for Sc(III)−salen are smaller than those observed in other

**TABLE 3: Coupled-Cluster Diagnostics from CCSD Calculations on the $1^1$A (Top), $1^3$A (Middle), and $1^5$A (Bottom) States of $3d^0$-Metal Salens**

| | T1(CCSD) | D1(CCSD) | T1/D1 |
|---|---|---|---|
| Sc(III) | 0.0202 | 0.0785 | 0.2573 |
| | 0.0402 | 0.2880 | 0.1396 |
| | 0.0369 | 0.2131 | 0.1732 |
| Ti(IV) | 0.0295 | 0.1318 | 0.2238 |
| | 0.0394 | 0.1870 | 0.2107 |
| | 0.0426 | 0.2642 | 0.1612 |
| V(V) | 0.1044 | 0.8323 | 0.1254 |
| | 0.0473 | 0.3227 | 0.1467 |
| | 0.0381 | 0.2039 | 0.1867 |
| Cr(VI) | 0.0738 | 0.4484 | 0.1646 |
| | 0.0450 | 0.2058 | 0.2185 |
| | 0.0746 | 0.4840 | 0.1541 |
| Mn(VII) | 0.0881 | 0.6620 | 0.1331 |
| | 0.0404 | 0.2143 | 0.1885 |
| | 0.0629 | 0.3597 | 0.1749 |

**TABLE 4: Leading Determinants in the Natural Orbital Basis from SA-CASSCF Calculations on the Low-lying Electronic States of Sc(III)−Salen**

| state | determinant | coeff |
|---|---|---|
| $1^1$A | $(R\pi_1)^2\,(R\pi_2)^2$ | 0.968 |
| $1^3$A | $(R\pi_1)^2\,(R\pi_2)\alpha(\mathrm{CN/CO}\pi_1^*)\alpha$ | 0.783 |
| | $(R\pi_1)^2\,(R\pi_2)\alpha(\mathrm{CN/CO}\pi_2^*)\alpha$ | 0.544 |
| | $(R\pi_2)^2\,(R\pi_1)\alpha(\mathrm{CN/CO}\pi_1^*)\alpha$ | 0.197 |
| $2^3$A | $(R\pi_2)^2\,(R\pi_1)\alpha(\mathrm{CN/CO}\pi_2^*)\alpha$ | 0.778 |
| | $(R\pi_2)^2\,(R\pi_1)\alpha(\mathrm{CN/CO}\pi_1^*)\alpha$ | −0.544 |
| | $(R\pi_1)^2\,(R\pi_2)\alpha(\mathrm{CN/CO}\pi_2^*)\alpha$ | −0.210 |
| $1^5$A | $(R\pi_1)\alpha(R\pi_2)\alpha(\mathrm{CN/CO}\pi_1^*)\alpha(\mathrm{CN/CO}\pi_2^*)\alpha$ | 1.000 |

**TABLE 5: Relative Energies (kcal mol$^{-1}$) for the Low-lying Electronic States of Ti(IV)−Salen Computed at Various Levels of Theory**

| | CCSD(T)[a] | CCSD[a] | MP2 | B3LYP | BP86 | BPW91 |
|---|---|---|---|---|---|---|
| $1^1$A | 0.00 | 0.00 | 344.93 | 0.00 | 0.00 | 0.00 |
| $1^3$A | 72.15 | 71.86 | 0.00 | 17.05 | 24.36 | 24.08 |
| $1^5$A | 107.82 | 99.21 | 82.17 | 51.68 | 66.57 | 65.80 |

[a] Relative energies computed at the MP2 optimized geometries.

transition-metal systems where CCSD(T) has been shown to provide reliable results.[88,89] On the other hand, the D1 diagnostics from Table 3 are considerably larger than the suggested cut-offs, indicating potential problems with the single-reference approximation. However, the small T1/D1 ratios indicate that the nondynamical effects may be well described by a relatively small active space (such as the four electron in four orbitals active space employed here). The leading determinants from the SA-CASSCF calculations presented in Table 4 clearly demonstrate the multireference nature of the electronic states. The leading coefficients for the triplet states (0.783 and 0.778 respectively) are both extremely small and the leading coefficient for the singlet state (at 0.968) is still smaller than what would be expected for a well-behaved single-reference system. Despite the demonstrated multireference character, all of the DFT approaches explored provide reasonable agreement to our high-level results for the geometries and relative energies of Sc(III)−salen.

**Ti(IV)—Salen.** The relative energies for Ti(IV)−salen are included in Table 5. The definition of an appropriate active space for accurately describing the low-lying electronic states of Ti(IV)−salen turned out to be considerably more challenging than for the other systems presented here. The increased formal oxidation state at the metal center results in the expected increased contribution of the metal d-orbitals. However, large CAS−CI computations at the BP86 $1^1$A geometry predict an electronic structure and active-space requirements very similar to that of Sc(III)−salen presented above. During the geometry optimization at the SA-CASSCF(4/4)/6-31G* [$1^1$A, $1^3$A, $2^3$A, $1^5$A] level, the CASSCF computations become highly unstable as the CN/CO$\pi$* orbitals begin to rotate in and out of the active space with the low-lying Ti(IV) d-orbitals. CAS−CI computations at this geometry reveal an increased contribution of the $d_{z^2}$, $d_{xz}$, and $d_{yz}$ orbitals as well as an increased number of low-lying electronic states. However geometry optimizations at the SA-CASSCF(4/7)/6-31G* [$1^1$A, $2^1$A, $3^1$A, $1^3$A, $2^3$A, $3^3$A, $1^5$A, $2^5$A] level were unsuccessful. Thus, the SA-CASSCF results for Ti(IV)−salen are not presented here.

All density functionals provide a qualitatively similar description of the electronic state ordering, being similar to that for Sc(III)−salen above with relatively smaller high-spin/low-spin splittings. The inclusion of HF exchange in the hybrid functional stabilizes the high-spin states slightly in comparison to BP86 and BPW91. Surprisingly, MP2 provides a highly unphysical description of the electronic state splittings, placing the $1^1$A state extremely high in energy. This is dramatically corrected at the coupled-cluster level, with CCSD and CCSD(T) providing similar results. However, even the CCSD(T) results are qualitatively very different from the DFT results. The large errors at the MP2 level require further investigation that will be discussed below. The results from DFT are in overall very good agreement with each other but they are very different from the CCSD(T) and the highly unphysical MP2 results. Overall, the BP86 and BPW91 results appear to give relative energies closer to CCSD(T), our best results for this system.

The T1 and D1 diagnostics from the CCSD computations on the $1^3$A and $1^5$A states of Ti(IV)−salen (see Table 3) are generally comparable to those from Sc(III)−salen discussed previously. However, the T1 and D1 diagnostics for the $1^1$A state are significantly larger (46% and 68% respectively) than the corresponding values for the Sc(III) system. While this signifies potentially larger nondynamical correlation effects, the smaller T1/D1 ratio indicates these may be well described by a relatively small active space. Returning to the results from single-reference approaches, the large errors from MP2 theory warrant further attention. Perturbation theory corrections for dynamical correlation are well-known to provide divergent results for certain chemical systems, especially as bonds are stretched far from equilibrium and small denominators arise from orbital near degeneracies. However, such effects are not typically observed for well-behaved systems at equilibrium geometries. Further examination reveals that the potential divergence of the perturbation correction is not the only source of the large errors provided by MP2 theory. The perturbation corrections are all of similar magnitude (−2.121269, −2.202915, and −2.297344 hartree for the $1^1$A, $1^3$A, and $1^5$A states respectively) and contribute to not more than 20% of the observed state splittings. The largest contributor to the errors in the spin-state splittings at the MP2 level in actuality is the HF reference energies. The RHF relative energies at the MP2 optimized geometries are highly unphysical: $1^1$A 293.70 kcal mol$^{-1}$, $1^3$A 0.0 kcal mol$^{-1}$, and $1^5$A 141.43 kcal mol$^{-1}$. Such effects have recently been observed, although to a slightly smaller extent, in other metal−salen systems. The oxo−Mn(salen) system has been demonstrated to possess multiple stable and unstable solutions to the self-consistent-field (SCF) equations, with HF theory providing highly unphysical splittings and being more susceptible to such solutions than DFT approaches.[27] In an effort to investigate such effects in Ti(IV)−salen, wave function stability analysis was performed on the $1^1$A RHF

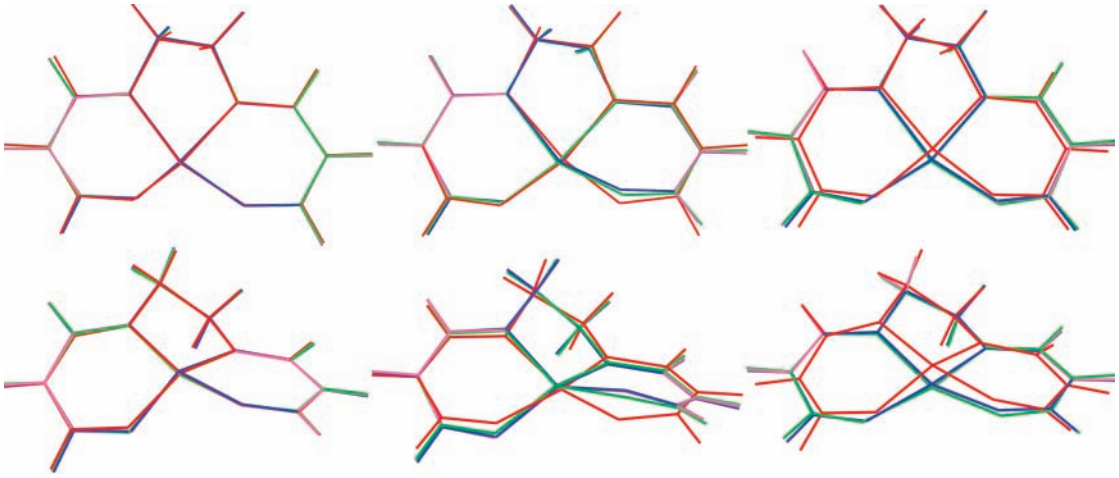

**Figure 6.** Overlay of the optimized geometries for the $1^1$A (left), $1^3$A (center), and $1^5$A (right) states of Ti(IV)−salen from different levels of theory. The theoretical methods include MP2 (red), B3LYP (green), BP86 (blue), and BPW91 (mauve).

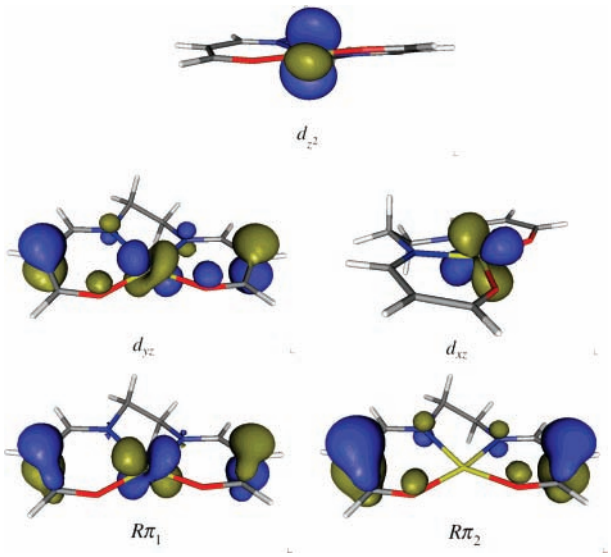


**Figure 7.** Isosurface plots of the $R\pi$ (bottom), $d_{yz}$ (middle-left), $d_{xz}$ (middle-right), and $d_{z^2}$ (top) orbitals that comprise the active space for V(V)−salen.

solution at the MP2 optimized geometry using Q-Chem 2.1[90,91] and an identical procedure as was employed in our previous work.[27] The closed-shell RHF reference solution is reproduced by all three choices of starting orbitals (core Hamiltonian, superposition of atomic densities, and Generalized Wolfsberg-Helmholtz) and furthermore, the $^1$A solution is shown to exhibit no RHF−RHF or RHF−UHF orbital instabilities. The smallest eigenvalue of the molecular orbital Hessian is found to be 0.0023. While this does not definitively rule out the existence of a stable RHF solution that is lower in energy, there is no straightforward procedure for locating such a solution. We are currently unable to perform stability analysis of the ROHF solutions for the $1^3$A and $1^5$A states and the existence of instabilities for these states would only serve to further exacerbate the highly unphysical description of the electronic state orderings at the HF−SCF level for Ti(IV)−salen.

The optimized geometries for Ti(IV)−salen are presented in Figure 6, and the LRMSD values are included in Table 2. While the geometries of the $1^1$A state are all very similar, the methods provide visibly different geometries for the $1^3$A and $1^5$A states. This is also clear from the LRMSD values in Table 2, where the LRMSD are more than twice as large for the $1^3$A and $1^5$A states. It is interesting to note the difference in the $1^3$A and $1^5$A geometries. For the $1^3$A state, the MP2 geometry is much more planar than those from the DFT approaches. In contrast, the MP2 geometry for the $1^5$A state exhibits significant out-of-plane puckering. Furthermore, the DFT geometries are much more planar for the $1^5$A state than is observed in the $1^3$A state. Overall, all of the DFT approaches perform similarly for the geometries of Ti(IV)−salen.

**V(V)—Salen.** In V(V)−salen the increased formal oxidation state at the metal center results in a larger d-orbital splitting that places the lowest d-orbitals energetically lower than the $\pi^*$ orbitals of the salen ligand. The lowest electronic states are dominated by $R\pi \rightarrow$ d excitations and appear to be adequately described by an active space consisting of the two $R\pi$ orbitals along with the $d_{z^2}$, $d_{xz}$, and $d_{yz}$ orbitals from the V(V) center, depicted in Figure 7. The SA-CASSCF(4/5)/6-31G*-[$1^1$A,$2^1$A,$1^3$A,$2^3$A,$1^5$A] relative energies are presented in Table 6. The CASPT3, CASPT2, and CASSCF results provide a consistent picture of the electronic structure for this system. As can be observed from the leading determinants in Table 7, the $1^1$A ground state and the low-lying $2^1$A state are open-shell singlet states with strong contributions from the metal d-orbitals. The lowest triplet state is predicted to lie less than 2 kcal mol$^{-1}$ above the ground state, with the $1^5$A state around 4.5 kcal mol$^{-1}$. Unlike in the previous systems, for V(V)−salen the density functionals provide a qualitatively different ordering of the low-

**TABLE 6: Relative Energies (kcal mol$^{-1}$) for the Low-Lying Electronic States of V(V)−Salen Computed at Various Levels of Theory**

| | CASPT3[a] | CASPT2[a] | CASSCF | CCSD(T)[b] | CCSD[b] | MP2 | B3LYP | BP86 | BPW91 |
|---|---|---|---|---|---|---|---|---|---|
| $1^1$A | 0.00 | 0.00 | 0.00 | 3.34 | 35.36 | 700.80 | 9.67 | 0.00 | 0.00 |
| $2^1$A | 3.73 | 2.21 | 2.42 | | | | | | |
| $1^3$A | 1.75 | 2.63 | 0.98 | 0.00 | 11.76 | 141.56 | 2.32 | 6.21 | 5.76 |
| $2^3$A | 3.12 | 4.97 | 2.07 | | | | | | |
| $1^5$A | 4.61 | 7.24 | 2.89 | 11.52 | 0.00 | 0.00 | 0.00 | 22.38 | 20.82 |

[a] Relative energies computed at the CASSCF optimized geometries. [b] Relative energies computed at the MP2 optimized geometries.

**TABLE 7: Leading Determinants in the Natural Orbital Basis from SA-CASSCF Calculations on the Low-Lying Electronic States of V(V)−Salen Computed at Their Optimized Geometries**

| state | determinant | coeff |
|---|---|---|
| $1^1$A | $(R\pi_1)^2\,(R\pi_2)\alpha(d_{yz})\beta$ | 0.4913 |
| | $(R\pi_1)^2\,(R\pi_2)\beta(d_{yz})\alpha$ | −0.4913 |
| | $(d_{xz})^2\,(R\pi_2)\alpha(d_{yz})\beta$ | −0.3663 |
| | $(d_{xz})^2\,(R\pi_2)\beta(d_{yz})\alpha$ | 0.3663 |
| $2^1$A | $(R\pi_1)^2\,(R\pi_2)\alpha(d_{z^2})\beta$ | 0.4962 |
| | $(R\pi_1)^2\,(R\pi_2)\beta(d_{z^2})\alpha$ | −0.4962 |
| | $(d_{xz})^2\,(R\pi_2)\alpha(d_{z^2})\beta$ | −0.3669 |
| | $(d_{xz})^2\,(R\pi_2)\beta(d_{z^2})\alpha$ | 0.3669 |
| $1^3$A | $(R\pi_1)^2\,(R\pi_2)\alpha(d_{yz})\alpha$ | 0.5774 |
| | $(R\pi_1)^2\,(R\pi_2)\beta(d_{xz})\alpha(d_{yz})\alpha$ | −0.4557 |
| | $(R\pi_1)^2\,(R\pi_2)\alpha(d_{xz})\alpha(d_{yz})\beta$ | 0.4436 |
| | $(d_{xz})^2\,(R\pi_1)\alpha(d_{yz})\alpha$ | −0.4368 |
| $2^3$A | $(R\pi_2)^2\,(R\pi_1)\alpha(d_{yz})\alpha$ | 0.5410 |
| | $(R\pi_1)^2\,(d_{xz})\alpha(d_{yz})\alpha$ | −0.5163 |
| | $(R\pi_2)^2\,(d_{xz})\alpha(d_{yz})\alpha$ | −0.4643 |
| | $(d_{xz})^2\,(R\pi_1)\alpha(d_{yz})\alpha$ | −0.4624 |
| $1^5$A | $(R\pi_1)\alpha(R\pi_2)\alpha(d_{xz})\alpha(d_{yz})\alpha$ | 0.9998 |

lying electronic states (see Table 6). Unsurprisingly perhaps, B3LYP predicts a high-spin $^5$A ground state while the GGA approaches accurately predict a $^1$A ground state. However, even the description provided from the BP86 and BPW91 functionals is qualitatively very different than that from our most accurate results, with both functionals placing the $1^5$A state considerably higher than the 4.6 kcal mol$^{-1}$ predicted at the CASPT3 level. The single-reference wavefunction-based approaches do not fare any better than the DFT results. As was observed for Ti(IV)−salen above, the HF reference dramatically over-stabilizes the high-spin states and provides an extremely challenging starting point from which to accurately describe the energetics of the system. The MP2 results predict the entirely wrong order of the electronic states with spin-state splittings that are unphysical and dramatically larger than the CASPT3 results, placing the $1^1$A state at 700.80 kcal mol$^{-1}$ relative to the $1^5$A state. Even coupled-cluster theory is unable to alleviate the large discrepancies in the HF reference energies, placing the $1^1$A state 35.36 and 3.34 kcal mol$^{-1}$ above the $1^5$A state at the CCSD and CCSD(T) levels, respectively.

The overall very poor performance of the single-reference approaches for V(V)−salen is not at all surprising given the weights of the leading determinants presented in Table 7 and the magnitude of the coupled-cluster diagnostics from Table 3. Both the singlet and triplet states are demonstrated to be highly multireference, with leading coefficients of 0.4913 and 0.4992 for the $1^1$A and $2^1$A states and 0.5774 and 0.5410 for the $1^3$A and $2^3$A states. The $1^5$A state appears to be strongly single-reference ($C_0 = 0.9998$) and this effect likely contributes to the dramatic over-stabilization of the $1^5$A state by HF-based approaches. The coupled-cluster diagnostics paint a similar picture, with T1's that are nearly twice the recommended critical values and D1's that are much larger than those from the previous systems. However, the T1/D1 ratios are actually smaller than those of Ti(IV)−salen and are very similar to those for the Sc(III) system. This bodes well for the applicability of similar-sized active spaces, being potentially smaller than those anticipated for the Ti(IV) system. Overall, both the coupled-cluster diagnostics and the CI vectors from the SA-CASSCF computations paint a similar picture of highly multireference $1^1$A and $1^3$A states and a single-reference $1^5$A state that are capable of being described by a small to modest active space.

Disappointingly, although it is probably of no surprise, the poor performance for relative energies by all single-reference approaches occurs simultaneously with decreased overall performance for molecular geometries. The LRMSD values relative to the CASSCF geometries presented in Table 8 are all several times larger than those observed in the seemingly well-behaved Sc(III)−salen and the geometries (overlaid in Figure 8) are visibly very different. As was observed in previous systems, the CASSCF geometries are much more planar than those from DFT, again with B3LYP geometries being closer to the CASSCF geometries than those from BP86 and BPW91. Contrary to the results observed previously, the MP2 geometries are closer to the B3LYP than to the CASSCF geometries. The

**TABLE 8: LRMSD(Å) in Molecular Geometries for the $1^1$A, $1^3$A, and $1^5$A States of (Lower Triangular) V(V)− and (Upper Triangular) Cr(VI)−Salens**

| | | CASSCF | MP2 | B3LYP | BP86 | BPW91 | | |
|---|---|---|---|---|---|---|---|---|
| | CASSCF | --- | 0.398 | 0.421 | 0.429 | 0.427 | CASSCF | |
| | | --- | 0.391 | 0.491 | 0.431 | 0.419 | | |
| | | --- | 0.486 | 0.486 | 0.605 | 0.615 | | |
| | MP2 | 0.783 | --- | 0.073 | 0.135 | 0.141 | MP2 | |
| | | 0.777 | --- | 0.234 | 0.180 | 0.174 | | |
| | | 0.769 | --- | 0.251 | 0.261 | 0.263 | | |
| V(V) | B3LYP | 0.865 | 0.319 | --- | 0.085 | 0.092 | B3LYP | Cr(VI) |
| | | 0.889 | 0.298 | --- | 0.100 | 0.115 | | |
| | | 0.784 | 0.450 | --- | 0.021 | 0.020 | | |
| | BP86 | 0.878 | 0.335 | 0.037 | --- | 0.141 | BP86 | |
| | | 0.933 | 0.372 | 0.095 | --- | 0.017 | | |
| | | 0.796 | 0.474 | 0.033 | --- | 0.005 | | |
| | BPW91 | 0.878 | 0.336 | 0.033 | 0.008 | --- | BPW91 | |
| | | 0.934 | 0.374 | 0.098 | 0.005 | --- | | |
| | | 0.796 | 0.477 | 0.035 | 0.005 | --- | | |

**TABLE 9: Relative Energies (kcal mol$^{-1}$) for the Low-lying Electronic States of Cr(VI)−Salen Computed at Various Levels of Theory**

| | CASPT3[a] | CASPT2[a] | CASSCF | CCSD(T)[b] | CCSD[b] | MP2 | B3LYP | BP86 | BPW91 |
|---|---|---|---|---|---|---|---|---|---|
| $1^1$A | 11.03 | 8.20 | 0.22 | 13.88 | 4.94 | 1282.36 | 31.62 | 16.81 | 18.61 |
| $1^3$A | 8.51 | 10.23 | 0.16 | 18.98 | 16.46 | 339.54 | 24.13 | 6.37 | 7.40 |
| $2^3$A | 9.93 | 12.78 | 1.98 | | | | | | |
| $1^5$A | 0.00 | 0.00 | 0.00 | 0.00 | 0.00 | 0.00 | 0.00 | 0.00 | 0.00 |

[a] Relative energies computed at the CASSCF optimized geometries. [b] Relative energies computed at the MP2 optimized geometries.

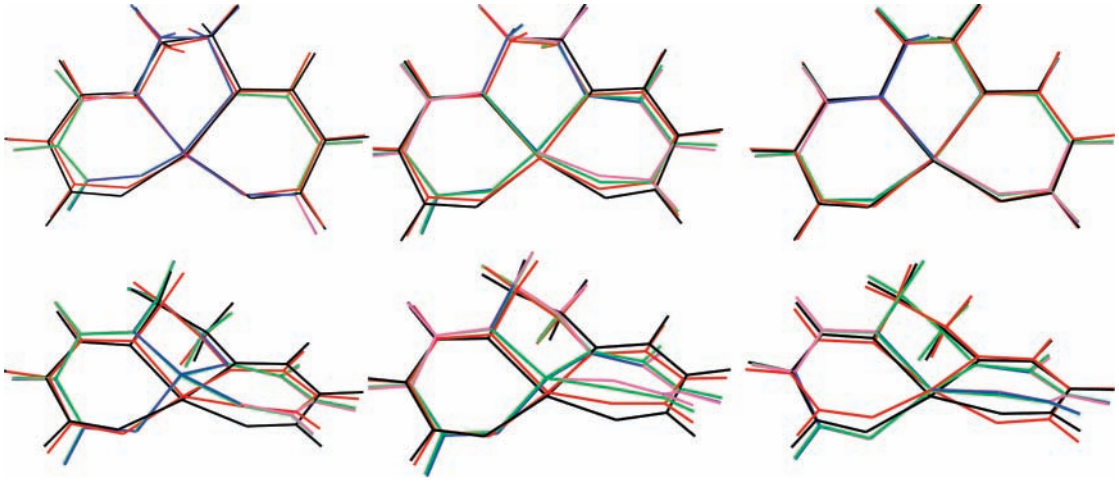

**Figure 8.** Overlay of the optimized geometries for the $1^1$A (left), $1^3$A (center), and $1^5$A (right) states of V(V)−salen from different levels of theory. The theoretical methods include CASSCF (black), MP2 (red), B3LYP (green), BP86 (blue), and BPW91 (mauve).

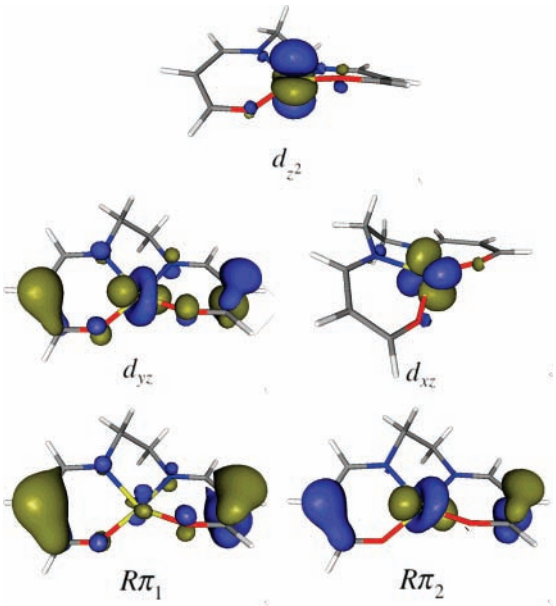


**Figure 9.** Isosurface plots of the R$\pi$ and Cr(d) orbitals that comprise the active space for Cr(VI)−salen.

LRMSD's for all methods approach 1 Å, being much larger than previously observed values.

**Cr(VI)—Salen.** CAS−CI computations on Cr(VI)−salen predict a similar active space (Figure 9) and electronic structure to that of V(V)−salen presented above. The SA-CASSCF(4/5)/6-31G*[$1^1$A, $1^3$A, $2^3$A, $1^5$A] relative energies are included in Table 9 along with those from CASPT2 and CASPT3. The lowest singlet, triplet, and quintet states are predicted to be nearly degenerate at the CASSCF level, with the $1^5$A ground state favored by no more than 0.22 kcal mol$^{-1}$. The inclusion of dynamical correlation stabilizes the $1^5$A state. At the CASPT2 level the $1^5$A state is predicted to be the ground state, with the $1^3$A and $1^1$A states at 10.23 and 8.20 kcal mol$^{-1}$ respectively. At the CASPT3 level these splittings are 8.51 and 11.03 kcal mol$^{-1}$. The MP2 results again appear highly unphysical, a consequence of the extremely poor description at the RHF level. Although we are currently incapable of performing stability analysis on the ROHF states, stability analysis was performed on the $1^1$A RHF solution. The RHF $1^1$A energy from ACES II is reproduced with Q-Chem for the three sets of starting orbitals. Exhibiting no RHF−RHF orbital instabilities, the lowest eigenvalue of the orbital Hessian (−0.0811) corresponds to a RHF−UHF instability. Following the instability leads to a heavily spin-contaminated ($\langle\hat{S}^2\rangle = 3.40$) UHF solution. The relative energies are dramatically improved at the CCSD and CCSD(T) levels, both being extremely different from the MP2 results. Even with the perturbative triples corrections, the CCSD(T) relative energies are still significantly different from the CASPT3 results. The relative energies for Cr(VI)−salen from all DFT approaches are also included in Table 9. All of the functionals predict a $1^5$A ground state, with B3LYP predicting much larger splittings than BP86 and BPW91. The predictions from DFT are in stark contrast to those from the multireference approaches presented above. While all methods accurately predict the $1^5$A ground state, the BP86 and BPW91 functionals predict smaller state splittings that are closer to our more reliable CASPT3 results.

**TABLE 10: Leading Determinants in the Natural Orbital Basis from SA-CASSCF Calculations on the Low-Lying Electronic States of Cr(VI)−Salen**

| state | determinant | coeff |
|---|---|---|
| $1^1$A | $(R\pi_1)^2\,(R\pi_2)\beta(d_{xz})\alpha$ | 0.4713 |
| | $(R\pi_1)^2\,(R\pi_2)\alpha(d_{xz})\beta$ | −0.4713 |
| | $(d_{yz})^2\,(R\pi_2)\alpha(d_{xz})\beta$ | 0.3577 |
| | $(d_{yz})^2\,(R\pi_2)\beta(d_{xz})\alpha$ | −0.3577 |
| | $(R\pi_1)\beta(R\pi_2)\alpha(d_{yz})\beta(d_{xz})\alpha$ | −0.2745 |
| | $(R\pi_1)\alpha(R\pi_2)\beta(d_{yz})\alpha(d_{xz})\beta$ | −0.2745 |
| | $(R\pi_1)^2\,(R\pi_2)^2$ | 0.1545 |
| $1^3$A | $(R\pi_1)^2\,(R\pi_2)\alpha(d_{xz})\alpha$ | 0.5310 |
| | $(d_{yz})^2\,(R\pi_2)\alpha(d_{xz})\alpha$ | −0.4362 |
| | $(R\pi_1)\alpha\,(R\pi_2)\alpha(d_{yz})\alpha(d_{xz})\beta$ | −0.3441 |
| | $(R\pi_1)^2\,(d_{yz})\alpha(d_{xz})\alpha$ | 0.3028 |
| | $(R\pi_2)^2\,(d_{yz})\alpha(d_{xz})\alpha$ | −0.2800 |
| | $(R\pi_2)^2\,(R\pi_1)\alpha(d_{xz})\alpha$ | −0.2362 |
| | $(d_{yz})^2\,(R\pi_1)\alpha(d_{xz})\alpha$ | 0.2095 |
| | $(R\pi_1)^2\,(R\pi_2)\alpha(d_{yz})\alpha$ | 0.1855 |
| $2^3$A | $(R\pi_2)^2\,(R\pi_1)\alpha(d_{xz})\alpha$ | 0.5020 |
| | $(R\pi_1)^2\,(d_{yz})\alpha(d_{xz})\alpha$ | −0.4904 |
| | $(R\pi_2)^2\,(d_{yz})\alpha(d_{xz})\alpha$ | 0.4459 |
| | $(d_{yz})^2\,(R\pi_1)\alpha(d_{xz})\alpha$ | −0.4340 |
| | $(R\pi_1)^2\,(R\pi_2)\alpha(d_{xz})\alpha$ | 0.1683 |
| $1^5$A | $(R\pi_1)\alpha(R\pi_2)\alpha(d_{yz})\alpha(d_{xz})\alpha$ | 1.0000 |

Upon examining the leading determinants from the CASSCF computations presented in Table 10 and considering the results presented previously for V(V)−salen, the rather poor performance of all single-reference approaches for Cr(VI)−salen should come of no surprise. The $1^1$A state is strongly open-shell in character and the closed-shell RHF determinant has a coefficient of only 0.1545. The triplet states are demonstrated

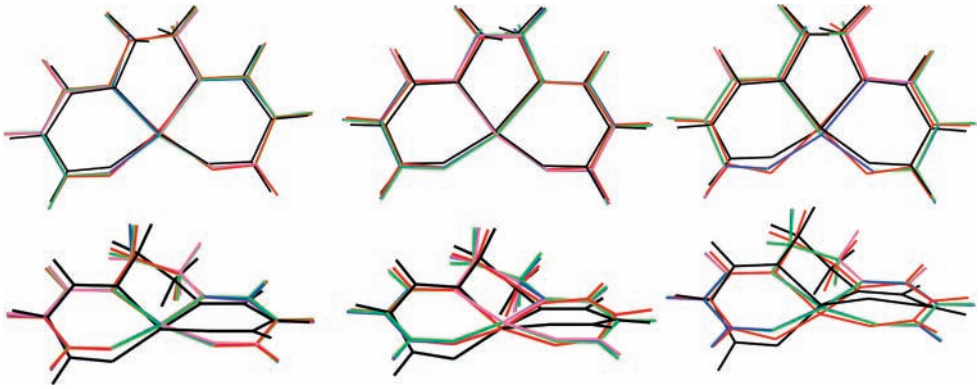

**Figure 10.** Overlay of the optimized geometries for the $1^1$A (left), $1^3$A (center), and $1^5$A (right) states of Cr(VI)−salen from different levels of theory. The theoretical methods include CASSCF (black), MP2 (red), B3LYP (green), BP86 (blue), and BPW91 (mauve).

to be strongly multireference as well, with leading coefficients of 0.5310 and 0.5020 for the $1^3$A and $2^3$A states respectively. In contrast to the singlet and triplet states, the $1^5$A appears strongly single-reference. The diagnostics from the CCSD computations (Table 3) are again much larger than what would be expected for well-behaved systems. Even CCSD(T) is incapable of overcoming the strong near-degeneracy effects present in Cr(VI)−salen.

The LRMSD in molecular geometries from all methods are presented in Table 8 and the optimized structures are overlaid in Figure 10. While the geometries are visibly very different, the LRMSD values from Table 8 are smaller than the corresponding values for V(V)−salen presented above. All of the DFT geometries are very similar, with a maximum LRMSD of 0.141 Å occurring between the BP86 and BPW91 $1^1$A geometries. The LRMSD values with respect to the CASSCF geometries are considerably larger, approaching 0.5 Å for all cases. The B3LYP geometries are overall somewhat closer to those from CASSCF than are the BP86 and BPW91 geometries, while the performance for relative energies is significantly better for the BP86 and BPW91 functionals.

**Mn(VII)—Salen.** For Mn(VII)−salen, the increased formal oxidation state at the metal center results in the four lowest-lying d-orbitals being energetically much lower than the salen $R\pi$ orbitals. Large CAS−CI computations indicate very little contribution from these orbitals to the low-lying electronic states. The 3 lowest electronic states were optimized at the SA-CASSCF(4/4)/6-31G*[$1^1$A, $1^3$A, $1^5$A] level using the active space depicted in Figure 11. The relative energies from all methods are included in Table 11. The DFT results are all very similar, with the anticipated stabilization of the high-spin $1^5$A state by B3LYP relative to BP86 and BPW91. The MP2 results are again completely unphysical. This is a consequesnce of the poor RHF description of the electronic structure of Mn(VII)−salen, although stability analysis of the RHF $1^1$A again confirms the lack of an RHF−RHF instability (there is a large RHF−UHF instability). As has been observed in the previous systems, CCSD dramatically improves upon the extremely poor MP2 results. However, it should be noted that the CCSD amplitude equations prove challenging to converge for many of the systems here. Often requiring hundreds iterations and fairly large level shifts, the amplitudes converge very slowly. Even with more than 300 iterations of the amplitude equations, the amplitudes failed to converge to the prescribed convergence criteria for the $1^3$A CCSD computation of Mn(VIII)−salen. The amplitudes in this case were converged to $10^{-7}$ which is slightly larger than the convergence criteria of $10^{-10}$. For this reason, the CCSD(T) energy for the $1^3$A state is omitted from Table 11. The CASSCF, CASPT2, and CASPT3 results provide a

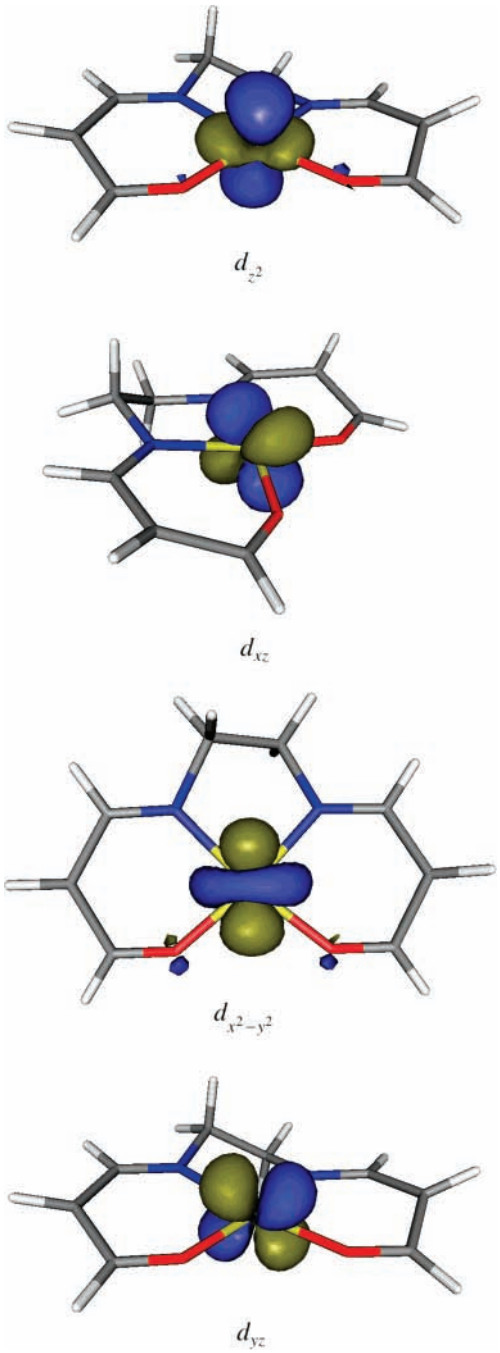


**Figure 11.** Isosurface plots of the Mn d-orbitals that comprise the active space for Mn(VII)−salen.

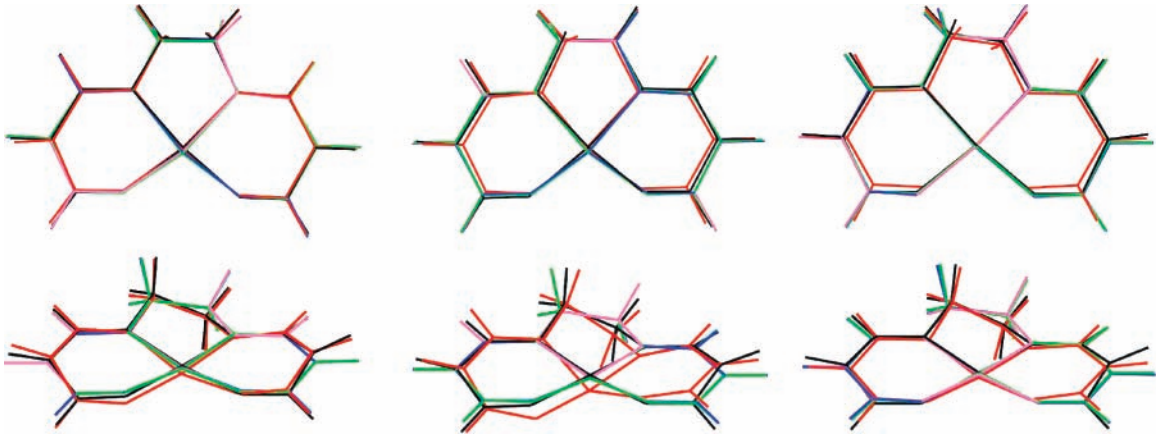

**Figure 12.** Overlay of the optimized geometries for the $1^1$A (left), $1^3$A (center), and $1^5$A (right) states of Mn(VII)−salen from different levels of theory. The theoretical methods include CASSCF (black), MP2 (red), B3LYP (green), BP86 (blue), and BPW91 (mauve).

**TABLE 11: Relative Energies (kcal mol$^{-1}$) for the Low-Lying Electronic States of Mn(VII)−Salen Computed at Various Levels of Theory**

| | CASPT3[a] | CASPT2[a] | CASSCF | CCSD(T)[b] | CCSD[b] | MP2 | B3LYP | BP86 | BPW91 |
|---|---|---|---|---|---|---|---|---|---|
| $1^1$A | 91.39 | 95.71 | 96.47 | 0.00 | 0.00 | 1709.09 | 54.35 | 33.83 | 37.33 |
| $1^3$A | 64.18 | 67.78 | 67.61 | | 10.52 | 598.78 | 35.73 | 16.35 | 18.77 |
| $1^5$A | 0.00 | 0.00 | 0.00 | 8.55 | 23.72 | 0.00 | 0.00 | 0.00 | 0.00 |

[a] Relative energies computed at the CASSCF optimized geometries. [b] Relative energies computed at the MP2 optimized geometries.

**TABLE 12: LRMSD(Å) in Molecular Geometries for the $1^1$A, $1^3$A, and $1^5$A States of Mn(VII)−Salen**

| | | CASSCF | MP2 | B3LYP | BP86 | BPW91 |
|---|---|---|---|---|---|---|
| | CASSCF | --- | | | | |
| | | --- | | | | |
| | | --- | | | | |
| | MP2 | 0.149 | --- | | | |
| | | 0.314 | --- | | | |
| | | 0.245 | --- | | | |
| Mn(VII) | B3LYP | 0.321 | 0.349 | --- | | |
| | | 0.313 | 0.483 | --- | | |
| | | 0.316 | 0.356 | --- | | |
| | BP86 | 0.333 | 0.358 | 0.026 | --- | |
| | | 0.327 | 0.495 | 0.030 | --- | |
| | | 0.362 | 0.410 | 0.060 | --- | |
| | BPW91 | 0.339 | 0.364 | 0.030 | 0.010 | --- |
| | | 0.326 | 0.493 | 0.028 | 0.006 | --- |
| | | 0.371 | 0.420 | 0.072 | 0.014 | --- |

consistent picture of the electronic state ordering in this system and are qualitatively very different from the CCSD and CCSD(T) results. Our best results place the $1^1$A and $1^3$A states at 91.39 and 64.18 kcal mol$^{-1}$ respectively relative to the $1^5$A ground state. The DFT relative energies provide reasonable (at least qualitative) agreement with the CASPT3 results, being dramatically better than the MP2 and CC results. Overall, the B3LYP relative energies are much closer to those from CASPT3 than are the other methods explored here.

The molecular geometries from all methods are overlaid in Figure 12, and the corresponding LRMSD values are presented in Table 12. While the DFT geometries agree very well with each other (LRMSD < 0.072 Å), the agreement with the CASSCF geometries is considerably worse (LRMSD > 0.313 Å). Despite the extremely poor performance of MP2 for the relative energies, the geometries from MP2 are closer to the CASSCF geometries than are the DFT geometries. However, with LRMSD values in excess of 0.149 Å, the geometries from MP2 and CASSCF remain noticeably different.

The leading determinants from the SA-CASSCF computations are presented in Table 13. The leading determinants for the $1^1$A and $1^3$A states are both extremely small (0.5977 and 0.8652 respectively), much smaller than would be expected for a single-reference system. It should be noted that, just as in the case of Sc(III)−salen, the $1^5$A state with this active space is a single determinantal wavefunction. The CC diagnostics from Table 3 reveal the same general trend, with the diagnostics being largest for the highly multireference $1^1$A state. The coefficients from the CASSCF computations and the CC diagnostics both demonstrate the incredibly strong multireference character of Mn(VIII)−salen. Surprisingly, the DFT approaches examined here outperform even CCSD(T) for this challenging system. The B3LYP results provide the closest agreement of the three functionals employed.

**TABLE 13: Leading Determinants in the Natural Orbital Basis from SA-CASSCF Calculations on the Low-Lying Electronic States of Mn(VII)−Salen Computed at Their Optimized Geometries**

| state | determinant | coeff |
|---|---|---|
| $1^1$A | $(d_{yz})^2\,(d_{x^2-y^2})^2$ | 0.5977 |
| | $(d_{xz})^2\,(d_{x^2-y^2})^2$ | −0.3816 |
| | $(d_{xz})^2\,(d_{z^2})^2$ | 0.3038 |
| | $(d_{x^2-y^2})^2\,(d_{z^2})^2$ | −0.3009 |
| | $(d_{yz})\beta(d_{x^2-y^2})\beta(d_{xz})\alpha(d_{z^2})\alpha$ | −0.2795 |
| | $(d_{yz})\alpha\,(d_{x^2-y^2})\alpha(d_{xz})\beta(d_{z^2})\beta$ | −0.2795 |
| | $(d_{yz})\beta(d_{x^2-y^2})\alpha(d_{xz})\beta(d_{z^2})\alpha$ | 0.2436 |
| | $(d_{yz})\alpha(d_{x^2-y^2})\beta(d_{xz})\alpha(d_{z^2})\beta$ | 0.2436 |
| $1^3$A | $(d_{x^2-y^2})^2\,(d_{yz})\alpha(d_{xz})\alpha$ | 0.8652 |
| | $(d_{z^2})^2\,(d_{yz})\alpha(d_{xz})\alpha$ | −0.4485 |
| $1^5$A | $(d_{z^2})\alpha(d_{x^2-y^2})\alpha(d_{yz})\alpha(d_{xz})\alpha$ | 1.0000 |

## Conclusions

Employing compact CASSCF reference spaces in conjunction with corrections for dynamical electron correlation at the CASPT3 level of theory, accurate relative energies and geometries have been obtained for the lowest electronic states of several $3d^0$-metal salen systems. The results presented clearly demonstrate the strong mult-reference character of the $3d^0$-metal salen systems explored. To the knowledge of the authors, the largest T1 and D1 diagnostics reported within this work exceed the largest values previously reported in the literature for

molecular systems at their respective equilibrium geometries.[92] The leading determinants from the SA-CASSCF computations serve to further validate this observation. Given the demonstrated strength of the nondynamical correlations in these systems, the poor performance of single-reference theories such as MP2, CCSD, and CCSD(T) when based upon a HF reference function may be of little surprise. Improvements can sometimes be made in the performance of coupled-cluster computations by abandoning the HF reference (consider the Brueckner coupled-cluster approaches as an example[93]). Future work will assess the importance of the choice of orbitals in coupled-cluster and multireference treatments of excited states in these and related molecular systems.

The DFT geometries and relative energies provide reasonable agreement with the benchmark results for two of the systems explored in this work: Sc(III) and Mn(VII). Interestingly, these are the systems possessing the smallest amount of mixing in the ligand $R\pi$ and the metal d-orbitals. For the case of Sc(III)−salen the electronic states are localized largely on the salen ligand. On the other hand, the electronic states are localized entirely on the metal center for the case of Mn(VIII)−salen. For the systems lying between these two extremes the DFT results are significantly worse. In these systems, the SA-CASSCF natural orbitals and determinants reveal a strong mixture of ligand $R\pi$ and metal d-orbital character in the lowest electronic states. Describing this appears to be a challenge for DFT approaches as the performance both for molecular geometries and for relative energies is degraded. However, it should be noted that all of the functionals examined perform approximately as well as the expensive CCSD(T) approach for these systems. While the hybrid functional does outperform BP86 and BPW91 for at least a couple of the cases examined, B3LYP is the only functional providing results in strong qualitative disagreement with any of the CASPT3 results. This is the case of V(V)−salen, where B3LYP fails to predict the $1^1$A ground state of the system. Given the strong multireference character of these systems, the overall reasonable qualitative and semiquantitative performance of the DFT approaches is surprising.

**Acknowledgment.** The authors thank the U.S. Department of Energy, Basic Energy Sciences, for financial support of this work through Catalysis Science Grant/Contract No. DE-FG02-03ER15459. The Center for Computational Molecular Science and Technology is funded through a Shared University Research (SUR) grant from IBM, by a CRIF grant from the NSF (CHE-0443564), and by Georgia Tech.

**Supporting Information Available:** Table of all of the coordinates for all states from the SA-CASSCF optimized geometries. This material is available free of charge via the Internet at http://pubs.acs.org.

## References and Notes

(1) Yoon, T. P.; Jacobsen, E. N. *Science* **2003**, *299*, 1691.
(2) Katsuki, T. *Adv. Synth. Catal.* **2002**, *344*, 131.
(3) Noyori, R. *Adv. Synth. Catal.* **2003**, *345*, 15.
(4) Blaser, H. U.; Spindler, F.; Studer, A. *Appl. Catal., A* **2001**, *221*, 119.
(5) Venkataramanan, N. S.; Kuppuraj, G.; Rajagopal, S. *Coord. Chem. Rev.* **2005**, *249*, 1249.
(6) McGarrigle, E. M.; Gilheany, D. G. *Chem. Rev.* **2005**, *105*, 1563.
(7) Canali, L.; Sherrington, D. C. *Chem. Soc. Rev.* **1999**, *28*, 85.
(8) Zheng, X. L.; Jones, C. W.; Weck, M. *Chem.—Eur. J.* **2005**, *12*, 576.
(9) Strassner, T.; Houk, K. N. *Org. Lett.* **1999**, *1*, 419.
(10) Khavrutskii, I. V.; Musaev, D. G.; Morokuma, K. *Proc. Natl. Acad. Sci. U.S.A.* **2004**, *101*, 5743.
(11) Jacobsen, H.; Cavallo, L. *Phys. Chem. Chem. Phys.* **2004**, *6*, 3747.
(12) Ivanic, J.; Collins, J. R.; Burt, S. K. *J. Phys. Chem. A* **2004**, *108*, 2314.
(13) Ivanic, J. *J. Chem. Phys.* **2003**, *119*, 9377.
(14) Abashkin, Y. G.; Collins, J. R.; Burt, S. K. *Inorg. Chem.* **2001**, *40*, 4040.
(15) Khavrutskii, I. V.; Musaev, D. G.; Morokuma, K. *Inorg. Chem.* **2005**, *44*, 306.
(16) Khavrutskii, I. V.; Rahim, R. R.; Musaev, D. G.; Morokuma, K. *J. Phys. Chem. B* **2004**, *108*, 3845.
(17) Khavrutskii, I. V.; Musaev, D. G.; Morokuma, K. *J. Am. Chem. Soc.* **2003**, *125*, 13879.
(18) Linde, C.; Arnold, M.; Norrby, P. O.; Akermark, B. *Angew. Chem., Int. Ed.* **1997**, *36*, 1723.
(19) Linde, C.; Akermark, B.; Norrby, P. O.; Svensson, M. *J. Am. Chem. Soc.* **1999**, *121*, 5083.
(20) Jacobsen, H.; Cavallo, L. *Chem.—Eur. J.* **2001**, *7*, 800.
(21) Cavallo, L.; Jacobsen, H. *Inorg. Chem.* **2004**, *43*, 2175.
(22) Cavallo, L.; Jacobsen, H. *J. Phys. Chem. A* **2003**, *107*, 5466.
(23) Cavallo, L.; Jacobsen, H. *J. Org. Chem.* **2003**, *68*, 6202.
(24) Cavallo, L.; Jacobsen, H. *Angew. Chem., Int. Ed.* **2000**, *39*, 589.
(25) Abashkin, Y. G.; Burt, S. K. *Org. Lett.* **2004**, *6*, 59−62.
(26) Brandt, P.; Norrby, P. O.; Daly, A. M.; Gilheany, D. G. *Chem.—Eur. J.* **2002**, *8*, 4299.
(27) Sears, J. S.; Sherrill, C. D. *J. Chem. Phys.* **2006**, *124*, 144314.
(28) Davidson, E. R. *Chem. Rev.* **1991**, *91*, 649.
(29) Kohn, W.; Sham, L. J. *Phys. Rev.* **1965**, *140*, 1133.
(30) Hohenberg, P.; Kohn, W. *Phys. Rev. B* **1964**, *136*, B864.
(31) Chermette, H. *Coord. Chem. Rev.* **1998**, *180*, 699.
(32) Cundari, T. R. *Computational organometallic chemistry*; Marcel Dekker: New York, 2001.
(33) Holthausen, M. C. *J. Comput. Chem.* **2005**, *26*, 1505.
(34) Yanagisawa, S.; Tsuneda, T.; Hirao, K. *J. Chem. Phys.* **2000**, *112*, 545.
(35) Barden, C. J.; Rienstra-Kiracofe, J. C.; Schaefer, H. F. *J. Chem. Phys.* **2000**, *113*, 690.
(36) Nakao, Y.; Hirao, K.; Taketsugu, T. *J. Chem. Phys.* **2001**, *114*, 7935.
(37) Harrison, J. F. *Chem. Rev.* **2000**, *100*, 679.
(38) Zhao, Y.; Truhlar, D. G. *J. Chem. Phys.* **2006**, *124*, 224105.
(39) Quintal, M. M.; Karton, A.; Iron, M. A.; Boese, A. D.; Martin, J. M. L. *J. Phys. Chem. A* **2006**, *110*, 709.
(40) Wang, S. G.; Schwarz, W. H. E. *J. Chem. Phys.* **1998**, *109*, 7252.
(41) Wodrich, M. D.; Corminboeuf, C.; Schleyer, P. V. *Org. Lett.* **2006**, *8*, 3631.
(42) Meermann, C.; Sirsch, P.; Tornroos, K. W.; Anwander, R. *J. Chem. Soc., Dalton Trans.* **2006**, 1041.
(43) Fukuzawa, S.; Komuro, Y.; Nakano, N.; Obara, S. *Tetrahedron Lett.* **2003**, *44*, 3671.
(44) Zhou, Z. H.; Li, Z. M.; Wang, Q. Y.; Liu, B.; Li, K. Y.; Zhao, G. F.; Zhou, Q. L.; Tang, C. C. *J. Organomet. Chem.* **2006**, *691*, 5790.
(45) Gregson, C. K. A.; Blackmore, I. J.; Gibson, V. C.; Long, N. J.; Marshall, E. L.; White, A. J. P. *J. Chem. Soc., Dalton Trans.* **2006**, 3134.
(46) Zhou, Z. H.; Wang, Q. Y.; Liu, B.; Zhao, G. F.; Zhou, Q. L.; Tang, C. C. *Lett. Org. Chem.* **2005**, *2*, 752.
(47) Ilyashenko, G.; Motevalli, M.; Watkinson, M. *Tetrahedron-Asymmetry* **2006**, *17*, 1625.
(48) Kim, S. S. *Pure Appl. Chem.* **2006**, *78*, 977.
(49) Belokon, Y. N.; Ishibashi, E.; Nomura, H.; North, M. *Chem. Commun.* **2006**, 1775.
(50) Belokon, Y. N.; Caveda-Cepas, S.; Green, B.; Ikonnikov, N. S.; Krustalev, V. N.; Larichev, V. S.; Moscalenko, M. A.; North, M.; Orizu, C.; Tararov, V. I.; Tasinazzo, M.; Timofeeva, G. I.; Yashkina, L. V. *J. Am. Chem. Soc.* **1999**, *121*, 3968.
(51) Khan, N. U. H.; Agrawal, S.; Kureshy, R. I.; Abdi, S. H. R.; Mayani, V. J.; Jasra, R. V. *Tetrahedron-Asymmetry* **2006**, *17*, 2659.
(52) Blacker, J.; Clutterbuck, L. A.; Crampton, M. R.; Grosjean, C.; North, M. *Tetrahedron-Asymmetry* **2006**, *17*, 1449.
(53) Ramon, D. J.; Yus, M. *Chem. Rev.* **2006**, *106*, 2126.
(54) Jaguar 5.5.; Schrödinger, L. L. C.: Portland, OR, 1991−2003.
(55) Becke, A. D. *Phys. Rev. A* **1988**, *38*, 3098.
(56) Perdew, J. P. *Phys. Rev. B* **1986**, *33*, 8822.
(57) Perdew, J. P.; Wang, Y. *Phys. Rev. B* **1992**, *45*, 13244.
(58) Becke, A. D. *J. Chem. Phys.* **1993**, *98*, 5648.
(59) Lee, C. T.; Yang, W. T.; Parr, R. G. *Phys. Rev. B* **1988**, *37*, 785.
(60) Chasman, D.; Beachy, M. D.; Wang, L. M.; Friesner, R. A. *J. Comput. Chem.* **1998**, *19*, 1017.
(61) Hay, P. J.; Wadt, W. R. *J. Chem. Phys.* **1985**, *82*, 270.
(62) Francl, M. M.; Pietro, W. J.; Hehre, W. J.; Binkley, J. S.; Gordon, M. S.; Defrees, D. J.; Pople, J. A. *J. Chem. Phys.* **1982**, *77*, 3654.

(63) Head-Gordon, M.; Pople, J. A.; Frisch, M. J. *Chem. Phys. Lett.* **1988**, *153*, 503.
(64) Stanton, J. F.; Gauss, J.; Watts, J. D.; Lauderdale, W. J.; Bartlett, R. J. *Int. J. Quantum Chem.* **1992**, 879.
(65) Roos, B. O.; Taylor, P. R. *Chem. Phys.* **1980**, *48*, 157.
(66) Werner, H. J.; Knowles, P. J.; Lindh, R.; Manby, F. R.; Schütz, M.; Celani, P.; Korona, T.; Rauhut, G.; Amos, R. D.; Bernhardsson, A.; Berning, A.; Cooper, D. L.; Deegan, M. J. O.; Dobbyn, A. J.; Eckert, F.; Hampel, C.; Hetzer, G.; Lloyd, A. W.; McNicholas, S. J.; Meyer, W.; Mura, M. E.; Nicklass, A.; Palmieri, P.; Pitzer, R.; Schumann, U.; Stoll, H.; Stone, A. J.; Trarroni, R.; Thorsteinsson, T.; MOLPRO 2006.1.
(67) Sherrill, C. D.; Schaefer, H. F. *Adv. Quantum Chem.* **1999**, *34*, 143.
(68) Pietro, W. J.; Hehre, W. J. *J. Comput. Chem.* **1983**, *4*, 241.
(69) Hehre, W. J.; Ditchfie. R.; Stewart, R. F.; Pople, J. A. *J. Chem. Phys.* **1970**, *52*, 2769.
(70) Hehre, W. J.; Stewart, R. F.; Pople, J. A. *J. Chem. Phys.* **1969**, *51*, 2657.
(71) Purvis, G. D.; Bartlett, R. J. *J. Chem. Phys.* **1982**, *76*, 1910.
(72) Raghavachari, K.; Trucks, G. W.; Pople, J. A.; Head-Gordon, M. *Chem. Phys. Lett.* **1989**, *157*, 479.
(73) Celani, P.; Werner, H. J. *J. Chem. Phys.* **2000**, *112*, 5546.
(74) Andersson, K.; Malmqvist, P. A.; Roos, B. O.; Sadlej, A. J.; Wolinski, K. *J. Phys. Chem.* **1990**, *94*, 5483.
(75) Werner, H. J. *Mol. Phys.* **1996**, *89*, 645.
(76) Humphrey, W.; Dalke, A.; Schulten, K. *J. Mol. Graphics Modell.* **1996**, *14*, 33.
(77) Portmann, S.; Luthi, H. P. *Chimia* **2000**, *54*, 766.
(78) Lee, T. J.; Taylor, P. R. *Int. J. Quantum Chem.* **1989**, 199.
(79) Lee, T. J. *Chem. Phys. Lett.* **2003**, *372*, 362.
(80) Ivanov, V. V.; Lyakhy, D. I.; Adamowicz, L. *Mol. Phys.* **2005**, *103*, 2131.
(81) Leininger, M. L.; Nielsen, I. M. B.; Crawford, T. D.; Janssen, C. L. *Chem. Phys. Lett.* **2000**, *328*, 431.
(82) Nielsen, I. M. B.; Janssen, C. L. *Chem. Phys. Lett.* **1999**, *310*, 568.
(83) Janssen, C. L.; Nielsen, I. M. B. *Chem. Phys. Lett.* **1998**, *290*, 423.
(84) Wissing, K.; Degen, J. *THEOCHEM* **1998**, *431*, 97.
(85) Messmer, R. P.; Interran. Lv.; Johnson, K. H. *J. Am. Chem. Soc.* **1974**, *96*, 3847.
(86) Rosch, N.; Messmer, R. P.; Johnson, K. H. *J. Am. Chem. Soc.* **1974**, *96*, 3855.
(87) Edmiston, C.; Ruedenberg, K. *Rev. Mod. Phys.* **1963**, *35*, 457.
(88) Peterson, K. A.; Figgen, D.; Dolg, M.; Stoll, H. *J. Chem. Phys.* **2007**, *126*, 124101.
(89) Peterson, K. A.; Shepler, B. C.; Singleton, J. M. *Mol. Phys.* **2007**, *105*, 445.
(90) Kong, J.; White, C. A.; Krylov, A. I.; Sherrill, D.; Adamson, R. D.; Furlani, T. R.; Lee, M. S.; Lee, A. M.; Gwaltney, S. R.; Adams, T. R.; Ochsenfeld, C.; Gilbert, A. T. B.; Kedziora, G. S.; Rassolov, V. A.; Maurice, D. R.; Nair, N.; Shao, Y. H.; Besley, N. A.; Maslen, P. E.; Dombroski, J. P.; Daschel, H.; Zhang, W. M.; Korambath, P. P.; Baker, J.; Byrd, E. F. C.; Van, Voorhis, T.; Oumi, M.; Hirata, S.; Hsu, C. P.; Ishikawa, N.; Florian, J.; Warshel, A.; Johnson, B. G.; Gill, P. M. W.; Head-Gordon, M.; Pople, J. A. *J. Comput. Chem.* **2000**, *21*, 1532.
(91) Shao, Y.; Molnar, L. F.; Jung, Y.; Kussmann, J.; Ochsenfeld, C.; Brown, S. T.; Gilbert, A. T. B.; Slipchenko, L. V.; Levchenko, S. V.; O'Neill, D. P.; DiStasio, R. A.; Lochan, R. C.; Wang, T.; Beran, G. J. O.; Besley, N. A.; Herbert, J. M.; Lin, C. Y.; Van Voorhis, T.; Chien, S. H.; Sodt, A.; Steele, R. P.; Rassolov, V. A.; Maslen, P. E.; Korambath, P. P.; Adamson, R. D.; Austin, B.; Baker, J.; Byrd, E. F. C.; Dachsel, H.; Doerksen, R. J.; Dreuw, A.; Dunietz, B. D.; Dutoi, A. D.; Furlani, T. R.; Gwaltney, S. R.; Heyden, A.; Hirata, S.; Hsu, C. P.; Kedziora, G.; Khalliulin, R. Z.; Klunzinger, P.; Lee, A. M.; Lee, M. S.; Liang, W.; Lotan, I.; Nair, N.; Peters, B.; Proynov, E. I.; Pieniazek, P. A.; Rhee, Y. M.; Ritchie, J.; Rosta, E.; Sherrill, C. D.; Simmonett, A. C.; Subotnik, J. E.; Woodcock, H. L.; Zhang, W.; Bell, A. T.; Chakraborty, A. K.; Chipman, D. M.; Keil, F. J.; Warshel, A.; Hehre, W. J.; Schaefer, H. F.; Kong, J.; Krylov, A. I.; Gill, P. M. W.; Head-Gordon, M. *Phys. Chem. Chem. Phys.* **2006**, *8*, 3172.
(92) DeYonker, N. J.; Peterson, K. A.; Steyl, G.; Wilson, A. K.; Cundari, T. R. *J. Phys. Chem. A* **2007**, *111*, 11269.
(93) Handy, N. C.; Pople, J. A.; Head-Gordon, M.; Raghavachari, K.; Trucks, G. W. *Chem. Phys. Lett.* **1989**, *164*, 185.